Vibrational spectrum of Ar_3^+ and relative importance of linear and perpendicular isomers in its photodissociation

František Karlický,[1,*] Bruno Lepetit,[2,3,†] René Kalus,[4] and Florent Xavier Gadéa[5,6]

[1]*Regional Centre of Advanced Technologies and Materials, Department of Physical Chemistry, Faculty of Science, Palacký University, Tř. 17. listopadu 12, 771 46 Olomouc, Czech Republic.*

[2]*Université de Toulouse, UPS, Laboratoire Collisions Agrégats Réactivité, IRSAMC, F-31062 Toulouse, France*

[3]*CNRS, UMR 5589, F-31062 Toulouse, France*

[4]*Department of Applied Mathematics, Faculty of Electrical Engineering and Computer Science, VSB - Technical University of Ostrava, 17. listopadu 15, 708 33 Ostrava, Czech Republic.*

[5]*Université de Toulouse, UPS, Laboratoire de Chimie et Physique Quantiques, IRSAMC, F-31062 Toulouse, France*

[6]*CNRS, UMR 5626, F-31062 Toulouse, France*

(Dated: January 26, 2011)

Abstract

The photodissociation dynamics of the argon ionized trimer Ar_3^+ is revisited in light of recent experimental results of (V. Lepère et al., J. Chem. Phys. **130**, 194301, 2009), which show that the fragment with little kinetic energy is always a neutral one, thus the available energy is shared by a neutral and ionic fragments, as in Ar_2^+. We show that these results can be interpreted as the photodissociation of the linear isomer of the system. We perform a 3D quantum computation of the vibrational spectrum of the system and study the relative populations of the linear (trimer-core) and perpendicular (dimer-core) isomers. We then show that the charge initially located on the central atom in the ground electronic state of the linear isomer migrates toward the extreme ones in the photoexcitation process, such that photodissociation of the linear isomer produces a neutral central atom at rest, in agreement with measured product state distributions.

PACS numbers: 33.20.-t, 33.20.Tp, 31.15.Ja, 34.80.Ht 36.40.-c, 36.40.Mr, 36.40.Wa

*Electronic address: `frantisek.karlicky@upol.cz`

†Electronic address: `bruno.lepetit@irsamc.ups-tlse.fr`

I. INTRODUCTION

Photofragmentation of ionic rare gas clusters have been studied extensively over the past decades both from theoretical and experimental points of view. One example of such systems is the argon ionic trimer Ar_3^+. On the theoretical side, structures of the different isomers of the system [1, 2], photodissociation [3–6] or photoabsorption spectra [7–10] were studied in details. On the experimental side, kinetic energy distributions of the photodissociation products have been measured [11–16], but it is only recently that complete information on products has been obtained using in coincidence detection of all ionic and neutral products ([17] and references therein). Indeed, measurement of the velocity vectors of all products allows reconstruction of the kinematics of the fragmentation. A complete description of the photodissociation dynamics of Ar_3^+ has been achieved for the first time in Ref. [17] for an excitation at 527 nm. Such results allow a more detailed comparison between experiments and models.

In the experimental results of Ref. 17, the dominant product configuration of the 3 body dissociation consists of a single fast neutral atom and a fast ion, the second neutral atom being left as a spectator with little kinetic energy. A strong similarity between this product configuration and the one obtained for the dimer photodissociation (in the UV range, however) is pointed out in Ref. 17, the main difference being the existence of the spectator atom in the trimer case. Another possible but less probable product configuration is one where the two neutral atoms bring away most of the available energy, little being left to the ionic fragment. These results have been interpreted in the light of the known theoretical results. In its electronic ground state, the trimer has linear and isosceles triangular isomers. The linear one is the most stable [1], its binding energy is 1.59 eV with respect to the $2Ar+Ar^+$ asymptotic limit (0.20 eV w.r.t. $Ar+Ar_2^+$), whereas the isosceles isomer binding energy is 1.47 eV (0.08 eV). The linear isomer has 50% of the charge on the central atom and 25% on each of the extreme atoms. The isosceles one is formed by a dimer ionic core, the charge being equally shared by its two atoms, the third atom at the principal vertex of the triangle being quasi-neutral. It is therefore concluded in Ref. [17] that the perpendicular isomer is the one which is observed in the coincidence experiment. The 2.35 eV energy deposited in the system leads primarily to the breaking of the strong bond (1.39 eV) of the Ar_2^+ ionic core, the excess energy, of about 0.86 eV, being released as kinetic energy of the

two fragments leaving the third particle, the spectator Ar atom, with a very small energy.

The aim of the present letter is to propose an alternative interpretation of the experimental results. Performing exact 3D quantum calculations on many excited vibrational states of Ar_3^+ and estimating the relative population of its two isomers, we show that the linear isomer is the one which is dominantly populated over a large temperature range. Then, from consideration of the charge distribution, not of the ground, but of the electronically excited states which are involved in the dissociation process, we show that photodissociation starting from the linear isomer is in full agreement with experimental results, in the sense that it produces a non-negligible amount of slow neutral fragments.

II. ISOMER POPULATIONS

The objective is to compare the relative populations of both isomers as a function of temperature. We first compute the vibrational partition function, which we then correct by inclusion of rotational effects. The vibrational states are computed from the extended (Ref. 18, 19) diatomics-in-molecules (DIM) model [20] developed previously [1, 10]. For simplicity, spin-orbit interaction is not taken into account in the present study which is not focused on high accuracy spectroscopy, but on a global estimate of the relative populations of the two isomers. This model leads to 9 electronic states, 6 of A' symmetry (among which we find the ground state) and 3 of A" symmetry with respect to the molecular plane (C_s group). For linear symmetric configurations, the ground state symmetry is Σ_u^+, and the excited states of interest in the energy range considered here have Π_u, Σ_g^+ and Π_g symmetries in increasing energy order. The vibrational energy spectrum is computed on the ground electronic potential energy surface using the row-orthonormal hyperspherical coordinates defined in Ref. 21. As this method has already been described in Ref. 22–25, we recall here only its most important features. The 6 degrees of freedom of the system in the center of mass frame are parametrized by a hyperradius ρ, which defines the global size of the system, and five angles collectively labeled by Ω. Three of them are Euler angles (a, b, c), which define the orientation of a body frame tied to the principal axes of inertia, and two additional angles θ and δ specifying the shape of the molecular triangle. These angles are defined in the intervals $\theta \in [0\,^\circ, 45\,^\circ]$ and $\delta \in [0\,^\circ, 180\,^\circ]$ (see Ref. 21). Linear configurations are obtained for $\theta = 0\,^\circ$, whereas $\theta = 45\,^\circ$ corresponds to the equilateral triangular configuration. Isosceles triangular

configurations are obtained when δ is a multiple of 30°. $\delta = 0\,^\circ, 60\,^\circ, 120\,^\circ$ correspond to obtuse isosceles configurations, where the principal vertex angle of the triangle is larger than 60°. Particular cases among these configurations are the linear symmetric ones obtained for $\theta = 0\,^\circ$. The 3 different values for δ correspond to the 3 possible choices for the central atom. $\delta = 30\,^\circ, 90\,^\circ, 150\,^\circ$ correspond to acute isosceles configurations. In these cases, when $\theta = 0\,^\circ$, 2 of the 3 atoms coincide.

The Hamiltonian reads:

$$H = -\frac{\hbar^2}{2\mu}\rho^{-5}\frac{\partial}{\partial\rho}\rho^5\frac{\partial}{\partial\rho} + \frac{\hat{\Lambda}^2}{2\mu\rho^2} + V(\rho,\theta,\delta), \tag{1}$$

where $\hat{\Lambda}$ is the grand canonical angular momentum, μ the 3-body reduced mass of the system, and $V(\rho,\theta,\delta)$ the ground state Born-Oppenheimer electronic potential energy. The nuclear wavefunction of the system, $\Psi_i^{JM\Pi}$, is labeled by the nuclear total angular momentum, J, its projection onto a space-fixed axis, M, and the parity, Π. i is the bound state number. $\Psi_i^{JM\Pi}$ is expanded on a product basis

$$\Psi_i^{JM\Pi}(\rho,\Omega) = \sum_{j,k} a_{jk}^i d_k(\rho)\Phi_j^{JM\Pi}(\Omega;\rho_k), \tag{2}$$

where $d_k(\rho)$ $(k = 1,\ldots,N_\rho)$ are discrete variable representation (DVR) functions [26, 27] which are obtained from a basis of sine functions on a regular grid of N_ρ grid points ρ_k in the interval $[\rho_{\min},\rho_{\max}]$. The N_s surface functions, $\Phi_j^{JM\Pi}$ $(j = 1,\ldots,N_s)$, are eigenfunctions of the fixed ρ Hamiltonian,

$$\left(\frac{\hat{\Lambda}^2}{2\mu\rho^2} + V(\rho,\theta,\delta)\right)\Phi_j^{JM\Pi}(\Omega;\rho) = \epsilon_j^{J\,\Pi}(\rho)\Phi_j^{JM\Pi}(\Omega;\rho), \tag{3}$$

and are needed only at the grid points, $\rho = \rho_k$. The coefficients a_{jk}^i of the expansion (Eq. 2) are obtained by diagonalizing the matrix representation of the Hamiltonian in the product basis, the size of which is $N_\rho N_s$. Notice that at a given grid point, ρ_l, Eq. 2 simplifies into

$$\Psi_i^{JM\Pi}(\rho_l,\Omega) = \sum_j a_{jl}^i \Phi_j^{JM\Pi}(\Omega;\rho_l). \tag{4}$$

Eq. 3 is solved by expanding the surface functions on a basis set of N_h principal-axes-of-inertia hyperspherical harmonics [28–30]. These harmonics are simultaneous eigenfunctions of the nuclear angular momentum operator, its projection on a space fixed axis, parity, as well as of the grand canonical angular momentum squared, $\hat{\Lambda}^2$, and of an internal hyperangular

momentum operator, $\hat{L} = -i\hbar\frac{\partial}{\partial\delta}$. These harmonics are generated on a 2 dimensional grid of $N_\theta \times N_\delta$ points.

This formalism can be used for any value of the total angular momentum, J, to compute high accuracy rovibrational spectra, as was done for instance in Ref. 23 for the neutral Ar_3 system. The present paper focuses on the vibrational spectrum for the case $J = 0$ (even parity Π) and incorporates rotational corrections in a subsequent step.

This spectrum should also correspond to a well defined permutation symmetry of the 3 identical nuclei. As argon has zero nuclear spin, the total electronuclear wavefunction must belong to the A_1 irreducible representation of the permutation group S_3. In the vicinity of equilateral triangular configurations, the ground electronic state forms a conical intersection with the first excited one which affects its nuclear permutation symmetry. Upon traversing a closed loop in nuclear configuration space around this conical intersection, the electronic wavefunction is changed to its opposite. The appropriate group to describe nuclear permutation properties of the electronic and nuclear components of the electronuclear wavefunction is the double group associated to S_3 and these two components each belong to the $\bar{A}_2$ irreducible representation (for a review on this topic, see Ref. 31). We therefore consider in the following $J = 0$ nuclear vibrational wavefunctions belonging only to the $\bar{A}_2$ irreducible representation of the permutation group.

Convergence parameters were tuned to obtain the 500 lowest vibrational energies with an absolute error less then 10^{-3} eV. This was achieved by comparing pairs of results involving the change of a single convergence parameter. Changing the number of angular grid points from $N_\theta = N_\delta = 200$ to 250 changed bound state energies by less than 10^{-6} eV. Changing the number of harmonics on which we expand the surface functions from $N_h = 1925$ to 3400 shifted these energies by less than 10^{-5} eV. Changing the number of surface functions from $N_s = 115$ to 230, or the number of grid points from $N_\rho = 64$ to 128, changed them by less than 10^{-4} eV. We therefore used the following input parameters in our calculations: $N_\theta = N_\delta = 200$, $N_h = 1925$, $N_s = 115$, $N_\rho = 64$. The hyperradius interval was bounded by $\rho_{\min} = 6.5$ a.u. and $\rho_{\max} = 13.5$ a.u. All calculations were performed with $M = 39.95$ u for the ^{40}Ar mass.

The surface function energy curves shown in Fig. 1 are the eigenvalues $\epsilon_i^{J=0\,\Pi=even}(\rho)$ of Eq. 3. Their shapes closely reflect the topology of the potential energy surface illustrated in Fig. 2 by means of polar plots for fixed ρ values (Fig. 2a) [32, 33]. The centers of these plots

correspond to equilateral triangular geometries, where the conical intersection between the two lowest potential energy surfaces is located. The minimum on surface function energy curves for $\rho = 7.85$ a.u. correspond to the three equivalent local minima of the potential energy surface associated to acute isosceles (T-shaped, C_{2v}) configuration. They are also shown as black dots in Fig. 2c, where the corresponding polar angles are 0° ($\delta = 90^\circ$) 120° ($\delta = 150^\circ$) or 240° ($\delta = 30^\circ$) for $\theta = 32.75\,^\circ$. The same character of the potential energy surface is preserved in short-range region too (Fig. 2b). The minima seen in Fig. 1 for $\rho = 9.05$ a.u. are associated to the three equivalent global minima corresponding to linear symmetric configurations (dots in Fig. 2e). The polar angles are 60° ($\delta = 120^\circ$), 180° ($\delta = 0^\circ$ or 180°) or 300° ($\delta = 60^\circ$) for $\theta = 0^\circ$. Transition states on reaction path between the linear and perpendicular isomers correspond to six equivalent saddle points for $\rho_{lim} = 8.82$ a.u. shown as dots in Fig. 2d. The corresponding polar angles are $[(k \cdot 120 \pm 39.20) \bmod 360]\,^\circ$ ($\delta = [(k \cdot 60 \pm 10.40) \bmod 180]\,^\circ, k = 1, 2, 3$) for $\theta = 23.04\,^\circ$. At large hyperradius ($\rho = 13$ a.u. in Figs. 1 and 2), one of the three atoms is far from the two others, the potential energy surface converges into the Ar_2^+ two body potential (potential valleys in Fig. 2f) and the surface function energies correlate to the rovibrational energies of the diatomics, Ar_2^+ (large ρ of Fig. 1). There is a transition in Fig. 1 near $\rho \approx \rho_{lim}$ where many weakly avoided crossings between different energy curves are observed. These are the result of a sudden change in the nature of the corresponding surface functions, from a perpendicular dominant character when $\rho < \rho_{lim}$ to a linear one at larger ρ. Another basis set alternative to the present surface function one could be a diabatic one, where true crossings can occur and where the character of the states, linear or perpendicular, would change more gradually with ρ. Instead of two minima, the corresponding energy curves would have a single one, which would be the linear or perpendicular one according to the character of the corresponding state.

Approximate quantum numbers can be assigned to the surface functions, following the methodology described in Ref. 24 for linear configurations and in Ref. 23 for perpendicular ones. For the linear case, the appropriate quantum numbers, v_a^l and $v_b^{l\,K}$, are associated to the antisymmetric stretch and bending vibrational modes. The vibrational angular momentum K is always 0 ($J = 0$) and v_b^l is constrained to be even. v_a^l is also even because we consider A_1 permutation symmetry [24]. The lowest surface functions energies minima at $\rho \approx 9.05$ a.u. correspond to $v_b^l = 0, 2, 4...$ and $v_a^l = 0$. As was shown in Ref. 24, only linear

states with even vibrational quantum numbers have to be considered, even in presence of a conical intersection. The surface functions minimum for larger ρ (the lowest one has a minimum near 9.25 a.u.) correspond to the antisymmetric stretch excitation ($v_a^l = 2$ for the lowest one). The perpendicular isomer can be described by the two quantum numbers v_a^p and v_b^p, where v_a^p refers to the vibration of the ionic Ar_2^+ core and v_b^p to the bending motion of the neutral Ar with respect to the ionic core. The electronic wavefunction being antisymmetric with respect to permutation of the atoms of the ionic core, the vibrational wavefunction also has to be antisymmetric (with respect to $\delta = \pi/2$) for the total electronuclear wavefunction to be symmetric. This enforces v_b^p to be odd. Notice, however, that the stretching motion (quantum number v_s^p) of Ar with respect to the ionic core is strongly mixed with bending motion in the hyperspherical representation. The series of potential energy curves spaced by roughly 0.01 eV with increasingly higher minima above $\rho \approx 7.85$ a.u. correspond to increasing v_b^p (mixed with v_s^p) for $v_a^p = 0$. The lowest potential energy curve for $v_a^p = 1$ has a minimum at $\rho = 7.85$ a.u. like the ground one, but is shifted upward by more than 0.03 eV.

The surface function basis is used to expand the wavefunction according to Eq. 2 and to generate a vibrational spectrum of 500 lowest states. The highest energy considered is -1.39 eV, the ground state corresponds to the linear isomer and its energy is -1.5877 eV. The lowest perpendicular isomer energy is 121.44 meV above this ground state. The vibrational zero point energies for linear and perpendicular energies are 26 and 32 meV respectively. A small subset of this spectrum is shown in Table I, as well as corresponding approximate vibrational quantum numbers. In an harmonic approximation, frequencies corresponding to different modes can be found out. For the linear isomer, these are 20, 7 and 17 meV (158, 56 and 136 cm^{-1}) for symmetric stretch, bending, and antisymmetric stretch modes, respectively. For the perpendicular isomer, these are 37 meV (298 cm^{-1}) for the vibration of Ar_2^+ ionic core, and 7 and 5 meV (60 and 45 cm^{-1}) for the stretch and bending motion of the third atom with respect to this core, respectively. Notice that the vibrational frequency of the core is only weakly affected by the presence of the third atom. Indeed, a vibrational frequency of 38 meV (306 cm^{-1}) has been extracted for ground electronic state Ar_2^+ from high resolution zero-kinetic-energy photoelectron spectra [34]. Recall also that nuclear spin and geometric phase constraints enforce bending quantum number to be even for the linear isomer and odd for the perpendicular one.

The energy difference between the ground states of the two isomers is large, 121.44 meV or

1415 K. This suggests that in experimental conditions not too far from thermal equilibrium, the linear isomer should be by far the most populated. This can be investigated further at thermal equilibrium by looking at the partition functions for both isomers. However, for sufficient excitation energy E_i, the bound state (number i) may be delocalized in the configuration space. Some criterion must be defined to assign a linear or perpendicular character to each state, e.g., a dividing surface between linear and perpendicular regions must be defined in configuration space, and linear and perpendicular weights w_i^l and w_i^p obtained as the presence probability of the bound state in each region. A temperature dependent population of the linear isomer can then be defined as $P_l(T) = \sum_i w_i^l e^{-E_i/(kT)}$, where k is the Boltzmann constant, and $P_p(T)$ can be defined similarly for the perpendicular isomer. We have already noticed previously a sharp transition for the surface functions from perpendicular to linear character near $\rho_{lim} = 8.82$ a.u., which corresponds to the transition state, so, we define the dividing surface by $\rho = \rho_{lim}$. Using Eq. 4 and integrating over hyperangles, we obtain

$$w_i^p = \sum_j \sum_{l\,:\,\rho_l < \rho_{lim}} a_{jl}^{i\,2} = 1 - w_i^l, \tag{5}$$

where the sum is performed over grid points l such that $\rho_l < \rho_{lim}$. Relative perpendicular population $P_p(T)/(P_l(T) + P_p(T))$ is depicted in Fig. 3 for 500 bound states. As expected, perpendicular isomer population is smaller than the linear one over a broad temperature range. This suggests that if experimental conditions are not too far from equilibrium in Ref. 17, the linear isomer should be the dominant one.

The limits of the results shown in Fig. 3 should be also considered. First, rotational effects have not been included. The simplest way to include them is to consider the rotational partition function in the approximation of rigid rotor for fixed geometries corresponding to the equilibrium geometries of both isomers in the classical limit. For the linear isomer and perpendicular isomers, these partition functions are : $Z_l(T) = \frac{1}{\sigma}\frac{2I}{\hbar^2}kT$ and $Z_p(T) = \frac{\pi^{\frac{1}{2}}}{\sigma}\left(\frac{2kT}{\hbar^2}\right)^{\frac{3}{2}}(I_1 I_2 I_3)^{\frac{1}{2}}$ [35]. I is the moment of inertia of the linear isomer, I_1, I_2 and I_3 those of the perpendicular one, $\sigma = 2$ the symmetry factor. The relative rovibrational perpendicular population obtained by multiplying the vibrational ones with rotational partition functions is also shown in Fig. 3. There is a strong increase of the relative perpendicular population induced by the larger value of the perpendicular partition function, as compared to the linear one. This in turn is due to the larger dimensionality of the parameter space for non linear

configurations (three Euler angles) as compared to the linear ones (2 angles). However, the smaller rotational space for linear isomer should be compensated by a larger vibrational space, resulting from the fact that bending occurs in a two dimensional space. This should be reflected in degeneracies of the vibrational modes which could be found out, either by computing the spectrum for a large number of non-zero angular momentum values or by assigning proper quantum numbers to all states of the spectrum. This, however, was not taken into account in our model, since for $J = 0$, the vibrational angular number is equal to 0 and both bending directions are excited in a similar fashion. In other words, we expect our relative perpendicular population without rotational correction to be closer to the true ro-vibrational one because it underestimates linear vibrational bending degeneracy and thus indirectly accounts for the larger rotational perpendicular partition function.

However, our definition of the dividing surface between linear and perpendicular zones is also subject to a discussion. One possibility would be to use a random walk method with importance sampling – wavefunction of Eq. 2 squared, as discussed in Ref. 36. An alternative definition would be based on the diabatic surface functions mentioned above which transform the sharply avoided crossings near ρ_{lim} into true crossings. Such surface functions would have a well defined perpendicular or linear character, and the coefficients of the expansion of the bound states on these states would provide their isomeric character. However, this diabatization would be technically difficult. One can anticipate that the resulting perpendicular relative population would be larger than the one obtained here. Such perpendicular diabatic surface functions would indeed extend for ρ values larger than ρ_{lim}. This larger importance of perpendicular isomers for higher temperatures is not surprising if we consider results from thermodynamics simulations of ionic rare gas trimers [2, 37]. It was found that the Ar_3^+ cluster is very stable in its linear ground state geometry up to about 300 K, and only then isomerizes to a T-shaped isomer in which a quasineutral atom moves around a charged dimer. As a result, our vibrational spectrum suggests dominance of the linear isomer unless very high temperatures are involved or the system is far from thermal equilibrium. Notice that under the experimental conditions of Ref. 17, the temperature is not clearly defined. Indeed, Ar_3^+ is obtained after ionization of large neutral clusters, followed by evaporative relaxation. This process leads to an ionized trimer at a not well defined rovibrational temperature, but probably with significant internal energy [38]. A more realistic way of the modeling of distributions of Ar_3^+ rovibronic states prior to photoexcitation,

namely injecting the output of post-ionization fragmentation simulations [39–43] into photodynamics calculations, is not possible at present due to the lack of relevant post-ionization fragmentation data and will require more extensive and detailed investigations in the future.

III. CHARGE MIGRATION IN PHOTOEXCITATION

We now concentrate on the photodissociation of the linear isomer and consider potentials, charges and transition dipole moments for slightly distorted configurations away from linearity ($\theta = 2\,^\circ$, $\delta = 1\,^\circ$; corresponding to the angles $173.07\,^\circ$, $3.36\,^\circ$, and $3.57\,^\circ$ of the molecular triangle). For such configurations, the states can be labeled by their exact symmetries (A' or A", C_s group) or approximate ones valid for strictly linear configurations ($D_{\infty h}$) [6–8, 10]. As shown in Fig. 4, the ground state is $A'(\Sigma_u^+)$, the first and second excited states are Π_u, the third one is Σ_g^+, and the fourth and fifth excited states are Π_g. However, in the Franck-Condon region, the only significant transition dipole moment is the one which connects the ground state to the Σ_g^+ one. Fig. 4b shows that for such transitions, charge localization on atoms is changed. Originally, about 50% of the positive charge is localized on the central atom, the remaining part being equally shared by the extreme atoms. Photoexcitation leads to a rearrangement of charges, such that all charge migrates to the extreme atoms, leaving the central atom neutral (Fig. 4b). This Σ_g^+ potential is strongly repulsive as a function of hyperradius and leads to direct dissociation of the trimer, where the extreme, now ionized atoms gain gradually kinetic energy and leave the central neutral atom essentially at rest. It is conceivable that electronic non-adiabatic couplings have some effect at large distance where the different potential energy surfaces are close to each other (Fig. 4a). These non-adiabatic couplings may mix the Σ_g^+ state with the other ones, bringing back some positive charge on the central atom. This could generate the small contribution observed in Ref. 17 with a slow ion and two fast neutrals. The fact that this contribution is small indicates that the charge back donation mechanism is not dominant and that the central atom, neutralized in the electronic excitation process, remains essentially in this state while dissociation takes place. This scenario was also the one predicted by many simulations on the photodissociation of Ar_3^+ when excited in the main visible band around 530 nm [3–9] and is fully compatible with experimental results of Ref. 17.

It should be also emphasized that the ionic dimer has an absorption band in the UV part

of the electromagnetic spectrum mainly while, here, a visible excitation is considered. For such energies, Franck-Condon factors favor excitation to the $^2\Pi_u$ state for the perpendicular isomer and Σ_g^+ for the linear case. However, as the dipole excitation from the ground $^2\Sigma_u^+$ state of Ar_2^+ to the $^2\Pi_u$ state is forbidden by symmetry, absorption from the perpendicular isomer is expected to be much weaker than the one of the parallel one. This is an additional reason for favoring the interpretation of the results of Ref. 17 in terms of photodissociation of the linear isomer.

IV. CONCLUSIONS

The recent detailed in coincidence measurements of the photodissociation of Ar_3^+ has led us to a reconsideration of the modeling of the process. We have presented a detailed analysis of the vibrational spectrum of the system and discussed the relative linear and perpendicular isomer populations. We have shown that under a wide range of experimental conditions, the linear isomer is likely to be the most populated. Although this isomer has a large positive charge on the central atom, photoexcitation leads to its neutralization, which means that the product of the photodissociation is a neutral atom essentially at rest and the charge is taken off by a fast ion. This model leads to an alternative interpretation of the experimental results of Ref. 17 which is compatible with the dominance of the linear isomer and which does not rest on the presumption of the key role of the perpendicular isomer.

V. ACKNOWLEDGMENTS

This work has been supported by the Barrande project (No. MEB020946), the Moravian-Silesian Region (mobility grant No. 13/2010), the Operational Program Research and Development for Innovations - European Social Fund (CZ.1.05/2.1.00/03.0058), and the Ministry of Education, Youth and Sports of the Czech Republic (grant No. MSM6198910027).

[1] D. Hrivňák and R. Kalus, Chem. Phys. **264**, 319 (2001).

[2] F. Calvo, F. X. Gadéa, A. Lombardi, and V. Aquilanti, J. Chem. Phys. **125**, 114307 (2006).

[3] F. X. Gadéa and M. Amarouche, Chem. Phys. **140**, 385 (1990).

[4] F. X. Gadéa and J. Durup, Laser Chem. **11**, 95 (1991).

[5] F. X. Gadéa, Z. Phys. D **20**, 25 (1991).

[6] A. Bastida and F. X. Gadéa, Z. Phys. D **39**, 325 (1997).

[7] F. X. Gadéa and M. Amarouche, J. Phys. II **5**, 1767 (1995).

[8] F. X. Gadéa and F. Lequere, J. Chem. Phys. **102**, 7830 (1995).

[9] A. Bastida and F. X. Gadéa, Chem. Phys. **209**, 291 (1996).

[10] J. Galindez, F. Calvo, P. Paška, D. Hrivňák, R. Kalus, and F. X. Gadéa, Comp. Phys. Commun. **145**, 126 (2002).

[11] A. B. Jones, A. L. M. Buxey, P. R. Jukes, J. A. Smith, and A. J. Stace, J. Chem. Phys. **103**, 474 (1995).

[12] H. Haberland, B. von Issendorf, and A. Hofmann, J. Chem. Phys. **103**, 3450 (1995).

[13] T. Nagata, J. Hirokawa, and T. Kondow, Chem. Phys. Lett. **176**, 526 (1991).

[14] T. Ikegami, T. Kondow, and S. Iwata, J. Chem. Phys. **93**, 3038 (1993).

[15] N. E. Levinger, D. Ray, K. K. Murray, A. S. Mullin, C. P. Schulz, and W. C. Lineberger, J. Chem. Phys. **91**, 4019 (1989).

[16] J. T. Snodgrass, C. M. Roehl, and M. T. Bowers, Chem. Phys. Lett. **159**, 10 (1989).

[17] V. Lepére, Y. J. Picard, M. Barat, J. A. Fayeton, B. Lucas, and K. Béroff, J. Chem. Phys. **130**, 194301 (2009).

[18] P. J. Kuntz and J. Valldorf, Z. Phys. D **8**, 195 (1988).

[19] M. Amarouche, G. Durand, and J. P. Malrieu, J. Chem. Phys. **88**, 1010 (1988).

[20] F. O. Ellison, J. Am. Chem. Soc. **85**, 3540 (1963).

[21] A. Kuppermann, J. Phys. Chem. **100**, 2621 (1996).

[22] B. Lepetit, R. Abrol, and A. Kuppermann, Phys. Rev. A **76**, 040702(R) (2007).

[23] F. Karlický, B. Lepetit, R. Kalus, and F. X. Gadéa, J. Chem. Phys. **126**, 174305 (2007).

[24] F. Karlický, B. Lepetit, R. Kalus, I. Paidarová, and F. X. Gadéa, J. Chem. Phys. **128**, 124303 (2008).

[25] L. Velilla, B. Lepetit, A. Aguado, J. A. Beswick, and M. Paniagua, J. Chem. Phys. **129**, 084307 (2008).

[26] O. Tolstikhin, S. Watanabe, and M. Matsuzawa, J. Phys. B : At. Mol. Opt. Phys. **29**, L389 (1996).

[27] J. Light and T. Carrington, Adv. Chem. Phys. **114**, 263 (2000).

[28] D. Wang and A. Kuppermann, J. Phys. Chem. A **107**, 7290 (2003).

[29] A. Kuppermann, J. Phys. Chem. A **110**, 809 (2006).

[30] B. Lepetit, D. Wang, and A. Kuppermann, J. Chem. Phys. **125**, 133505 (2006).

[31] F. Bouakline, B. Lepetit, S. Althorpe, and A. Kuppermann, Springer Series in Chemical Physics **97**, 201 (2009).

[32] Polar plots are used such that the distance to the center of each plot is proportional to $\pi/2 - 2\theta$ and the polar angle is given by $(2\delta - \pi)$ mod 2π. This produces plots consistent with the usual equatorial projection of the internal configuration space [33]. The center of the polar plot ($\theta = \pi/4$) corresponds to equilateral triangular configurations, the outer circle ($\theta = 0$) corresponds to linear configurations. On this circle (see Fig. 2a.), the three equivalent points corresponding to polar angles 0 ($\delta = \pi/2$), $2\pi/3$ ($\delta = 5\pi/6$), and $4\pi/3$ ($\delta = \pi/6$) are singular points where two of the three atoms coincide.

[33] R. Abrol and A. Kuppermann, J. Chem. Phys. **116**, 1035 (2002).

[34] R. Signorell, A. Wüest, and F. Merkt, J. Chem. Phys. **107**, 10819 (1997).

[35] G. Herzberg, *Infrared and Raman spectra of polyatomic molecules* (Krieger, 1991).

[36] C. A. Brindle, M. R. Prado, K. C. Janda, N. Halberstadt, and M. Lewerenz, J. Chem. Phys. **123**, 064312 (2005).

[37] R. Kalus, D. Hrivňák, and A. Vítek, Chem. Phys. **325**, 278 (2006).

[38] V. Lepére, private communication.

[39] A. Bastida, N. Halberstadt, J. A. Beswick, F. X. Gadéa, U. Buck, R. Galonska, and C. Lauenstein, Chem. Phys. Lett. **249**, 1 (1996).

[40] D. Bonhommeau, N. Halberstadt, and A. Viel, J. Chem. Phys. **124**, 184314 (2006).

[41] I. Janeček, D. Hrivňák, R. Kalus, and F. X. Gadéa, J. Chem. Phys. **125**, 104315 (2006).

[42] F. Calvo, D. Bonhommeau, and P. Parneix, Phys. Rev. Lett. **99**, 083401 (2007).

[43] I. Janeček, S. Cintavá, D. Hrivňák, R. Kalus, M. Fárník, and F. X. Gadéa, J. Chem. Phys. **131**, 114306 (2009).

TABLE I: Vibrational energy levels and approximate quantum numbers, for linear and perpendicular isomers. The reference energy is the one of the ground state, which lies 1,5877 eV below the energy of the fully dissociated configuration Ar^++Ar+Ar. v_s^l, v_b^l, v_a^l are the symmetric, bending, and antisymmetric stretch vibrational quantum numbers of the linear isomer. K is the vibrational angular momentum ($K = 0$ since $J = 0$). For the perpendicular isomer, v_a^p is the vibrational quantum number of the Ar_2^+ ionic core, and v_s^p,v_b^p describe stretching and bending of the 3^{rd} atom with respect to this core. Several states referred to as "..." are omitted in the list for the perpendicular isomer to show the first ionic core excitation ($v_a = 1$).

Linear isomer		Perpendicular isomer	
Energy (meV)	v_s^l,$v_b^{l\,K}$,v_a^l	Energy (meV)	v_s^p,v_b^p,v_a^p
0.	$0\,0^0\,0$	121.44	0 1 0
13.88	$0\,2^0\,0$	128.93	1 1 0
19.59	$1\,0^0\,0$	132.66	0 3 0
27.55	$0\,4^0\,0$	135.88	2 1 0
33.35	$1\,2^0\,0$	138.65	1 3 0
33.67	$0\,0^0\,2$	141.94	3 1 0
39.58	$2\,0^0\,0$	143.07	0 5 0
41.03	$0\,6^0\,0$	144.47	2 3 0
46.11	$0\,2^0\,2$	...	...
46.92	$1\,4^0\,0$	158.83	0 1 1

Figure captions

Fig. 1 Surface function potential energy curves $\epsilon_i^{J=0\,\Pi=0}(\rho)$ as a function of the hyperradius (see Eq. 3), for the ground electronic potential energy curve of Ar_3^+.

Fig. 2 Topology of the electronic ground-state PES of Ar_3^+ shown for five representative hyperradii in an equatorial view (see Fig. 1 of Ref. 33). Plots are polar ones, the distance to the center of each plot is proportional to $\pi/2 - 2\theta$ and the polar angle is given by $(2\delta - \pi)$ mod 2π. (a) General scheme of trimer configurations for a fixed value of ρ; (b) $\rho = 7.00$ a.u. (short-range region); (c) $\rho = 7.85$ a.u. (local minimum region, dots are located at the three equivalent local minima on the PES corresponding to acute isosceles C_{2v} configurations); (c) $\rho = 8.82$ a.u. (transition state region, dots are located at the six equivalent transition states of the system corresponding to asymetric configurations); (c) $\rho = 9.05$ a.u. (global minimum region, dots are located at the three equivalent absolute minima on the PES corresponding to linear symmetric configurations); (d) $\rho = 13.00$ a.u. (asymptotic, long-range region where one atom is far from the two others). All energies are given in eV, the zero of energy corresponds to the fully dissociate state, $Ar^+ + 2Ar$.

Fig. 3 The relative population of the perpendicular isomer of Ar_3^+ at thermal equilibrium as a function of temperature. The curve labelled "No rot" results from the partition functions computed from the $J = 0$ vibrational spectrum, the one labelled "Rot" includes the correction of the rotational partition functions.

Fig. 4 Potential energy (a), charge on the middle atom (b), and transition dipole momentum squared (c) of six lowest electronic states of Ar_3^+ as a function of hyperradius ρ. The considered geometry is $\theta = 2\,^\circ$, $\delta = 1\,^\circ$, close but not exactly linear, corresponding to the molecular triangle angles $173.07\,^\circ$, $3.36\,^\circ$, and $3.57\,^\circ$.

FIG. 1:

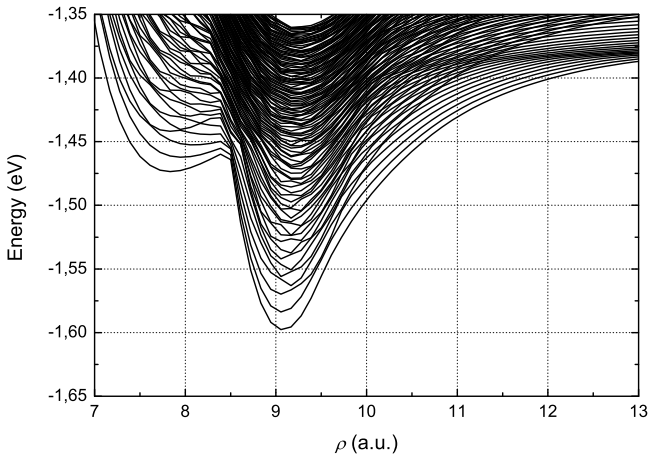

FIG. 2:

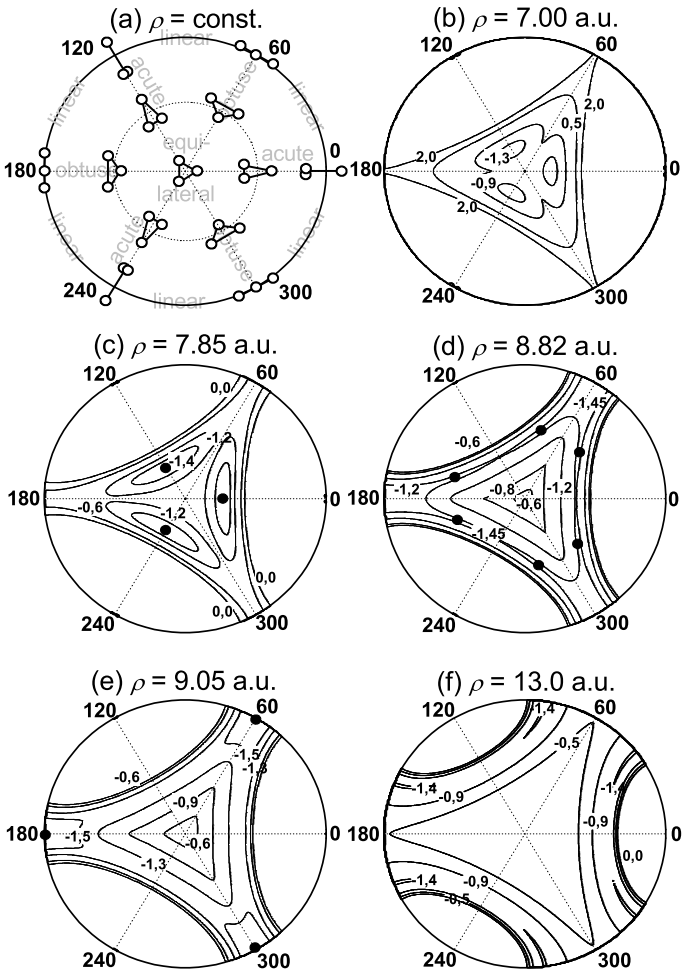
(a) ρ = const.
linear
acute
obtuse
linear
acute
obtuse
linear
obtuse
acute
linear
acute
obtuse
linear
equi
lateral
acute
120
60
180
0
240
300
(b) ρ = 7.00 a.u.
2,0
0,5
-1,3
-0,9
2,0
2,0
(c) ρ = 7.85 a.u.
0,0
-1,2
-1,4
-0,6
-1,2
0,0
0,0
(d) ρ = 8.82 a.u.
-1,45
-0,6
-1,2
-0,8
-0,6
-1,2
-1,45
(e) ρ = 9.05 a.u.
-1,5
-1,3
-0,6
-0,9
-1,5
-0,6
-1,3
(f) ρ = 13.0 a.u.
1,4
-0,5
-1,4
-0,9
-0,9
0,0
-1,4
-0,9
-0,5

FIG. 3:

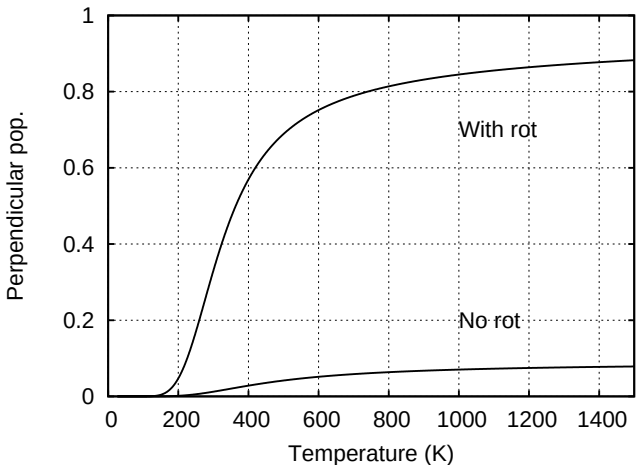
Perpendicular pop.
Temperature (K)
With rot
No rot
0
0.2
0.4
0.6
0.8
1
0
200
400
600
800
1000
1200
1400

FIG. 4:

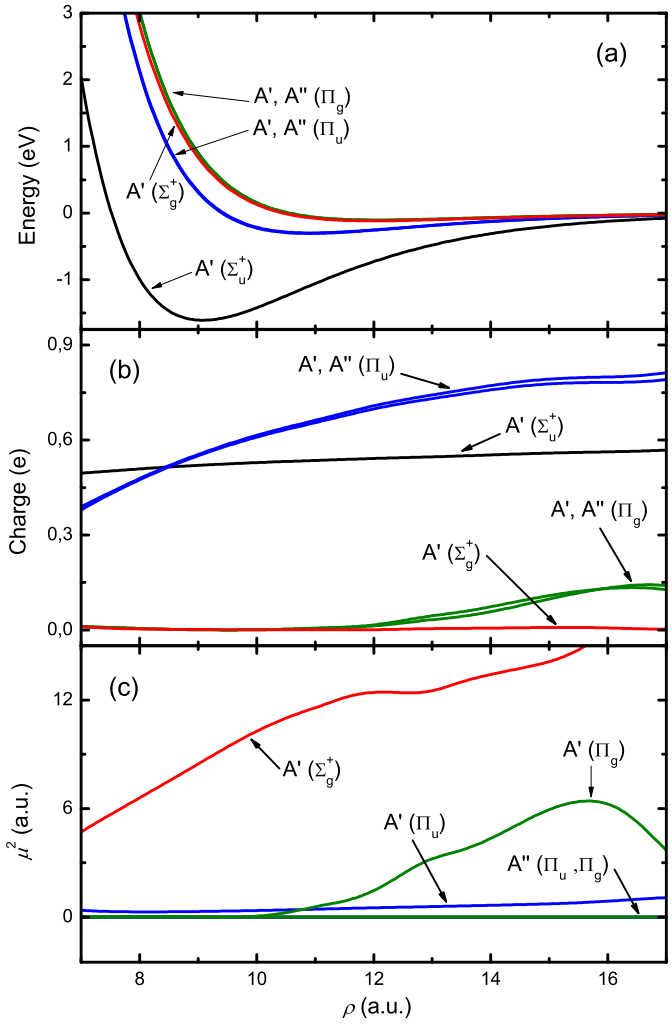
(a)
Energy (eV)
A', A'' (Π_g)
A', A'' (Π_u)
A' (Σ_g^+)
A' (Σ_u^+)
(b)
Charge (e)
A', A'' (Π_u)
A' (Σ_u^+)
A', A'' (Π_g)
A' (Σ_g^+)
(c)
μ^2 (a.u.)
A' (Σ_g^+)
A' (Π_g)
A' (Π_u)
A'' (Π_u ,Π_g)
ρ (a.u.)